



# **Journal of Geophysical Research: Atmospheres**

# **RESEARCH ARTICLE**

10.1002/2016JD026442

#### **Kev Points:**

- Determines the TRMM electrified cloud parameters that have the best joint seasonal-diurnal correlation to the global electric circuit
- Finds the differences in the measured GEC between the two ENSO phases.
  Distinct differences can be seen in the GEC between the two phases
- Determined that similar patterns of seasonal-diurnal variation as the GEC can be seen in the TRMM parameters during the two phases of ENSO

#### Correspondence to:

T. Lavigne, tlavigne@islander.tamucc.edu

#### Citation:

Lavigne, T., C. Liu, W. Deierling, and D. Mach (2017), Relationship between the global electric circuit and electrified cloud parameters at diurnal, seasonal, and interannual timescales, *J. Geophys. Res. Atmos.*, 122, 8525–8542, doi:10.1002/2016JD026442.

Received 29 DEC 2016 Accepted 7 AUG 2017 Accepted article online 11 AUG 2017 Published online 23 AUG 2017

# Relationship between the global electric circuit and electrified cloud parameters at diurnal, seasonal, and interannual timescales

Thomas Lavigne<sup>1</sup> (D), Chuntao Liu<sup>1</sup> (D), Wiebke Deierling<sup>2</sup> (D), and Douglas Mach<sup>3</sup> (D)

<sup>1</sup>Department of Physical and Environmental Sciences, Texas A&M University, Corpus Christi, Texas, USA, <sup>2</sup>Department of Aerospace Engineering Sciences, University of Colorado Boulder, Boulder, Colorado, USA, <sup>3</sup>Science and Technology Institute, Universities Space Research Association, Huntsville, Alabama, USA

Abstract In the early 1900s, J. W. Whipple began to validate C. T. R. Wilson's global electric circuit (GEC) hypothesis by correlating the diurnal variation of global thunder days with the diurnal variation of the fair weather electric field measured by the Carnegie Cruise. This study applies 16+ years of precipitation feature (PF) data from the Tropical Rainfall Measuring Mission, including lightning data from the Lightning Imaging Sensor, alongside 12 years of electric field measurements from Vostok, Antarctica, to further examine this relationship. Joint diurnal-seasonal variations of the electric field are introduced and compared with a variety of PF parameters that are potentially related to the GEC. All tested PF parameters showed significant correlations to the electric field on the joint seasonal-diurnal timescale, with the flash rate and volume of 30 dBZ between the  $-5^{\circ}$ C and  $-35^{\circ}$ C isotherms showing the best linear correlations with  $R^{2}$  values of 0.67 and 0.62, respectively. Furthermore, these relationships are analyzed during the two different phases of the El Niño-Southern Oscillation. Results show different seasonal-diurnal variations of the electric field during El Niño and La Niña periods, with enhancements in the electric field between the months of January through April at 16–24 UTC in La Niña years. A similar trend is shown in global PF parameters, indicating relationships between the variations seen in the fair weather electric field and the variations of global PFs at diurnal, seasonal, and interannual timescales. This provides further evidence that PFs around the globe have a direct connection to the GEC.

### 1. Introduction

The global electric circuit (GEC) of the atmosphere is a naturally occurring phenomenon in which air acts as a very weak conductor between the ionosphere and the Earth's surface [Roble and Tzur, 1986; Markson, 2007; Williams, 2009]. It has long been hypothesized that electrified clouds, including those with or without thunder, act as the driver or "battery" to sustain the fair weather electric field of the GEC [Wilson, 1920; Williams, 2009]. During the past century, the mechanisms of electric charge separation inside these "batteries" (thunderstorms and electrified shower clouds) have been gradually revealed based on laboratory and field experiments. As early as the beginning of the twentieth century, J. W. Whipple made the critical connection between the diurnal variation of thunder days around the globe and the diurnal variation of the fair weather electric field [Whipple, 1929]. More recent work has verified this claim with airborne and satellite observations and emphasized the importance of the role electrified shower clouds play in the GEC [Mach et al., 2009, 2010, 2011; Liu et al., 2010; Blakeslee et al., 2014a].

Precipitation-based charging, involving rebounding collisions between ice particles (e.g., pristine ice crystals and graupel), has been shown to be the major mechanism of charge separation inside the cloud [Reynolds et al., 1957; Takahashi, 1978; Takahashi and Miyawaki, 2002, Saunders, 2008]. This separation of charge inside a thunderstorm is supported by the noninductive charging theory and is strengthened by observations connecting the volume and mass of radar sensitive ice particles with total (intracloud and cloud-to-ground) lightning flash rate [Carey and Rutledge, 1996; MacGorman et al., 2005; Liu et al., 2012 and many others]. Previous studies have concluded that the region and conditions most suitable for charge separation occurs between the temperatures of  $-10^{\circ}$ C and  $-20^{\circ}$ C, with at least 1-3 g/m $^3$  of cloud water content in the cloud [Takahashi, 1978]. Furthermore, graupel-sized particles have been determined to be extremely important in the charge separation process [Workman and Reynolds, 1950]. It has been determined that a significant amount of charge separation occurs in the presence of the combination of ice crystals, graupel, and super cooled

©2017. American Geophysical Union. All Rights Reserved.



liquid water all combined in the cloud [Takahashi, 1978; Saunders and Peck, 1998; Deierling et al., 2008]. The charge separation per collision increases rapidly with increasing ice crystal size [Keith and Saunders, 1990]. Several studies have been conducted to compare the vertical structure of radar reflectivity and storm dynamical properties as well as a combination to storm total amount of lightning. Deierling et al. [2008] studied a series of field campaigns over varying types of storms using dual-polarimetric dual-Doppler radar data to estimate the ice mass fluxes. Precipitation and nonprecipitation ice mass flux estimations were found to correlate well to the lightning flash rate with a correlation coefficient of 0.93 [Carey and Rutledge, 1996; Deierling et al., 2008]. Petersen et al. [2005] used TRMM observations and found that TRMM PR-derived ice water path correlates well with flash densities. More recently, Liu et al. [2012] compared vertical structure radar reflectivity to the flash rate over the entire tropics and subtropics using the TRMM satellite. A high correlation between flash rate and area and volume of high radar reflectivity was found in the mixed-phase region in the PFs between -5°C and -35°C [*Liu et al.*, 2012].

There have been numerous past studies on the diurnal and seasonal variation of the GEC [Williams and Heckman, 1993; Williams, 1994; Adlerman and Williams, 1996; Blakeslee et al., 2014a]. The consensus is that the fair weather electric field follows the trends in global storm activity and has a maximum in the northern hemisphere summer months [Adlerman and Williams, 1996]. This tends to support the "storm theory" of the GEC, providing more evidence correlating global electrified clouds to the electric field. However, more research is needed to understand the quantitative relationships between seasonal and interannual variations of the GEC and global electrified clouds.

The El Niño-Southern Oscillation (ENSO) is a known natural variation in the Earth's climate [Rasmusson and Wallace, 1983]. El Niño is defined as abnormally warm sea surface temperatures, weakened easterly trade winds, and increased rainfall over the equatorial East Pacific [Chronis et al., 2008]. The effects of the ENSO variability can influence general circulation and regional distributions of precipitation and convection around the entire tropics and subtropics. For example, the enhancement of the Walker circulation [Julian and Chervin, 1978] under the La Niña scenario may lead to the suppression of convection over the eastern Pacific and more active convection over the Maritime Continent. Theoretically, assuming that all else stays equal, the GEC should respond to this changing of the occurrence and distribution of convection [Williams and Mareev, 2014]. Recent work using the TRMM Lightning Imaging Sensor (LIS) and Optical Transient Detector shows that seasonal thunderstorm activity has a significant correlation with ENSO [Dowdy, 2016]. The Maritime Continent, Northeast Brazil, Western North Pacific, and the Gulf of Mexico were all shown to have high correlation between seasonal lightning activity and ENSO. Another study conducted at the Lerwick Observatory in the UK's Shetland Islands, compared the measured electric field in that region to the corresponding ENSO time periods [Harrison et al., 2011]. The results revealed an increase in El Niño electric fields compared to La Niña or neutral phases in sea surface temperature. This result corresponds directly to the past work that has been done on the variations in lightning activity with the ENSO cycle and gives direct evidence that variations in global circulation patterns are also reflected in the electric field measurements. It is the general consensus that the global lightning flash count increases in the warmer El Niño conditions [Sátori and Zieger, 1999; Hamid et al., 2001; Satori et al., 2009; Williams, 2009; Dowdy, 2016]. A recent study conducted over the Indonesian region shows a significant increase in lightning activity over the islands during El Niño conditions [Hamid et al., 2001]. These findings give support for the understanding that the GEC and global thunderstorms are indeed somehow correlated and connected on the ENSO timescale. Williams and Mareev [2014] claim that more research is needed on this subject to definitively correlate the ENSO cycle with the GEC. The motivation of this work is to answer the following questions:

- 1. Which properties of precipitation systems that are related to the charge separation process follow similar diurnal and seasonal variations as the fair weather electric field?
- 2. Are there any differences in the measured fair weather electric field values between El Niño and La Niña
- 3. Can these same differences be seen in the properties of precipitation systems as well?

To answer these questions, this study builds upon past research, but with much more complete and robust data sets due to modern electric field measurements and the use of satellite data. Section 2 covers the data retrieval and possessing methodology for the two sets of data collected. Section 3.1 introduces the joint seasonal and diurnal variations of the electric field and compares this variation to the variation seen in



cloud properties on the same timescales. Section 3.2 then introduces the importance of the relationship between the El Niño-Southern Oscillation (ENSO) and the electric field and compares cloud feature parameters to the measured electric field in both the positive and negative phases of the ENSO cycle. Section 4 discusses the long-standing discrepancy between the timing of the maxima of global lightning compared to the maxima in the GEC. Section 5 then summarizes the findings.

# 2. Data and Methodology

#### 2.1. Electric Field Measurements From Vostok, Antarctica

This study uses 12 years of surface electric field measurements taken from Vostok Station, Antarctica, during two separate field campaigns spanning 1998-2004 and 2007-2011 [Burns et al., 2005, 2012]. This location provides very high quality electric field measurements because of the stably stratified boundary layer that guarantees suppressed convective overturn, with the exception of a few hours around local noon in the summer months [Burns et al., 2005, 2017; Williams, 2009]. This condition eradicates much of the weather influences that have the ability to contaminate fair-weather electric field conditions and mask a global signal. In addition, the majority of the surface of the East Antarctic Plateau is flat, reducing the impact of wind turbulence. At Vostok Station, electric field measurements were taken every 10 s and averaged into 1 min intervals over the duration of the campaigns [Burns et al., 2005]. On the surface, the average fair weather electric field is approximately 100 V/m. However, these values are expected to double over the Antarctic plateau due to very little radioactivity, and therefore lower conductivity and lower column resistance [Markson, 2007]. The influences on the fair weather electric field can be from storm activity, high winds, solar radiation influences, solar wind, and a wide array of other interferences [Tinsley, 2000]. Other previous work studying the cross polar cap potential over the Antarctic plateau shows an approximate 15% decrease in the measured electric field at Vostok Station in the 3 days following interplanetary magnetic field (IMF) sector boundaries [Frank-Kamenetsky et al., 1999; Corney et al., 2003; Burns et al., 2005]. Comparisons of the vertical electric field measured at Vostok have been made with the Weimer 1996 model of the cross polar cap potentials, revealing statistical correlations at all UTC hours with the most significant correlations occurring around Vostok's local magnetic noon of 13 UTC [Burns et al., 2005]. To remove the local weather influence, electric field measurements that are potentially impacted by local weather were removed if values are above 350 V/m and below 46 V/m. For any values that exceeded 350 V/m, data recorded 2 h before and after the event were also removed from the analysis. Based on Burns et al. [2005], over the course of a 4 year study (1998–2001), these measurements were determined to be the maximum and minimum fair-weather values in Vostok. For ease of data processing, all remaining measurements are considered to be "fair weather" values and are included in the manuscript. Comparison of the joint seasonal-diurnal variation of the extended 12 year period after removal of locally influenced electric field measurements results in nearly identical variation patterns as observed in [Burns et al., 2005] (figure not shown). For this analysis, the IMF influence was not removed. After a comparison to the results of the second Vostok field campaign [Burns et al., 2012], we found that the simple weather filtering without considering IMF led to an average electric field value of 2.5% lower than if the IMF influence was considered. However, the comparison of the joint seasonal and diurnal variations of the simple weather filtered values, and corrected IMF values in Burns et al. [2012], shows a correlation coefficient of 0.98, indicating almost identical seasonal and diurnal variation patterns observed by both techniques (figure not shown).

It is important to point out the difference in fair weather electric field values between the two campaigns. The mean fair-weather value of the first field campaign was 195 V/m, while the mean fair weather electric field of the second campaign was of 157 V/m. The measurements taken from Vostok are relative and not absolute measurements [Burns et al., 2012]. There was no calibration done relative to the steel pole that the field mill was mounted on, and the two campaigns could have had different measurement heights or configurations leading to the discrepancy between the two sets of data. Despite the varying mean electric field values between campaigns, the diurnal and seasonal variation patterns of the electric field remain very similar. Therefore, the relative and not absolute variations are emphasized in this study. To demonstrate the original data set, the electric field data collected during the two separate campaigns are combined to create a single longer-running time series of the electric field over Vostok. The mean value of the Vostok electric field therefore represents the mean over the entire 12 year period. For this study, the electric field variation observed on the interannual, seasonal, and diurnal timescales are of more importance when comparing to the properties



of global electrified clouds, in comparison to the magnitude of the electric field values themselves. It is also important to point out that it is very difficult to account for all the local influences at the station during the time of data collection. Recent work comparing simultaneous measurements taken from Vostok and Concordia stations in Antarctica shows that it is very rare for simultaneous measurements at the two sites separated by 560 km to be matched [Burns et al., 2017]. This being said, the one 5 day sequence of measurements at both sites in Antarctica showed highly correlated behavior. Furthermore, in the same study, dozens of individual days with highly correlated simultaneous electric field measurements were taken from both sites. This provides more evidence that the data set is indeed globally representative for at least the diurnal variation.

#### 2.2. Properties of Precipitation Features

This study uses 16+ years (1998–2014) of precipitation feature data from the Tropical Rainfall Measuring Mission (TRMM) satellite [Nesbitt and Zipser, 2000; Liu et al., 2008]. With TRMM, lightning flashes are recorded onboard via the Lightning Imaging Sensor (LIS). The vertical structures of precipitation systems are measured with the Ku band radar on the TRMM satellite. Precipitation features (PFs) are defined as near-surface groupings of adjacent pixels where precipitation was observed by the TRMM precipitation radar [Liu et al., 2008]. Although there are nearly 75% of PFs with an area of less than 75 km<sup>2</sup>, their total contribution to rainfall is less than 5% over the TRMM domain [Liu et al., 2010]. Most of these small PFs are also shallow and oceanic Liu and Zipser, 2009. The total rainfall contribution from PFs with area less than 75 km<sup>2</sup> and radar echo top reaching 4.5 km (about 0°C) is only 0.6%. To ease data processing, any PFs containing less than 75 km<sup>2</sup> are excluded in this manuscript. Observed precipitation for the context of this manuscript is defined as contiguous area of at least 75 km<sup>2</sup> with rain rate of at least 0.1 mm/h based on the TRMM 2A25 rainfall retrieval algorithm [lguchi et al., 2000]. In general, charge separation inside a cloud requires two main conditions to occur: (1) The PFs must contain adequately large-sized ice particles, and (2) PFs must reach above the 0° isotherm, and thus, ice/super cooled liquid water must be present. Typically, precipitation systems that produce graupel and hail particles in the mixed phased region yield ideal conditions for charge separation and electrification to occur [Takahashi and Miyawaki, 2002; Liu et al., 2012]. For this reason, quantifying the area and volume of 30 dBZ above  $-5^{\circ}$ C as well as the ice water content for each PF in the mixed phase region can be a useful proxy for charge separation. It is important to note that not all PFs that meet these before mentioned conditions produce lightning. This is why it is imperative to include all thunderstorms as well as electrified shower clouds, when observing the GEC. Electrified shower clouds are defined as PFs with area greater than 75 km<sup>2</sup> that have 30 dBZ at  $-10^{\circ}$ C with no lightning flashes over land and 30 dBZ at  $-17^{\circ}$ C over the ocean [Liu et al., 2010]. These electrified clouds are herein defined as any PF that meets at least one requirement for being electrified, such as either fulfilling the definition of being an electrified shower cloud or having at least one lightning flash as seen by the TRMM LIS. Total rainfall from electrified PFs is then defined as the total rainfall from thunderstorms combined with the total rainfall from electrified shower clouds. For comparison, total rainfall from all PFs and those over land are also analyzed.

It is important to point out the caveats of using the PF data set in this study. The TRMM satellite provides only a "snapshot" of each PF of approximately one and half minutes or more depending on the size of the PF. A thunderstorm with a flash rate less than 0.6 flashes per minute can be misclassified as an electrified shower cloud. At the same time, electrified shower clouds embedded in a multiple cell systems with thunder could be misclassified as a thunderstorm PF. In this way, many electrified shower clouds are subsets of thunderstorm PFs and thus undercounted. Therefore, it is impossible to definitively determine the classification of each PF into thunderstorms or electrified shower clouds. Electrified shower clouds may also be undercounted due to the exclusion of PFs with a size smaller than 75 km<sup>2</sup>. Therefore, the relative contributions to the electric field from thunderstorms and electrified shower clouds cannot be exactly quantified with the PF data set without further constraints. Here we focus on the variations of the properties of all PFs, including both thunderstorms and electrified shower clouds, at different timescales.

All parameters in this study are measured in the TRMM coverage domain from 36°N to 36°S in latitude covering the tropics and subtropics. For all seasons other than northern hemisphere summer, TRMM observes about 90% of the global lightning [Christian et al., 2003]. In the northern hemisphere summer, TRMM misses approximately 30% of global lightning, mainly from the northern mid-high latitudes [Christian et al., 2003]. Parameters are chosen to relate to the electric field due to their physical ties to the charge separation in



clouds as shown in previous studies [Liu et al., 2010, 2012]. For this study, new parameters have also been introduced in order to better represent the physical properties behind the charge separation. Occurrence of 30 dBZ in the mixed phase region is defined as the volume of 30 dBZ between  $-5^{\circ}$ C and  $-35^{\circ}$ C divided by the total sampled volume observed by TRMM between  $-5^{\circ}$ C and  $-35^{\circ}$ C. Rainfall from electrified PFs includes rainfall from both thunderstorms and electrified shower clouds, although the definitive separation between the two types of PFs is impossible. All other rainfall that is observed from PFs that do not meet the definition of either a thunderstorm or electrified shower cloud are considered from nonelectrified clouds. The global mean flash rate is calculated to represent the total number of lightning strikes per second seen at any given time in the TRMM domain. All parameters have been normalized to account for the sampling bias in the TRMM orbit after dividing by the total number of TRMM sampled pixels to remove the oversampling around 32° latitudes resulting from the latitudinal maxima of the orbital track.

# 2.3. El Niño-Southern Oscillation (ENSO) Month Selections

As stated previously, the El Niño–Southern Oscillation (ENSO) has two distinct phases [*Trenberth*, 1997]. The warm phase, which is known as El Niño, is classified as abnormally warm sea surface temperatures in the eastern Pacific Ocean. La Niña is the cold phase, which is classified as abnormally cool sea surface temperatures in this region. A running 3 month mean of the Oceanic Niño Index (ONI) [*Yu et al.*, 2010] was used to determine the phase of each sampled month. The ONI index is a measurement of the sea surface temperature anomaly in the region of (5°N–5°S and 120°W–170°W). According to this ONI index, a month is considered either an El Niño or La Niña month, if the variation from the normal sea surface temperature has at least a 0.5°C deviation from the mean. Following this index, all El Niño years included in this paper have at least an ONI index of at least +0.5 and all La Niña years have an index value of at most –0.5. It is important to note that this classification technique makes no distinction between very strong and weak ENSO events.

#### 3. Results

In past studies, global lightning and thunderstorm parameters have been compared to the yearly mean diurnal variation curve of the fair weather electric field or Carnegie Curve [Whipple, 1929; Williams and Heckman, 1993; Markson, 2007; Williams, 2009; Liu et al., 2010; Mach et al., 2011]. The focus has traditionally been on the diurnal amplitude and phase after removing the mean values. Although this type of comparison is valuable, it does not necessarily provide as much detail into the seasonal dependence of the UTC diurnal cycle. Furthermore, a one-to-one linear relationship may not be present between the PF parameters and the electric field. For these reasons, it may be more valuable to analyze the trends and patterns in a joint seasonal and diurnal analysis.

# 3.1. Joint Seasonal and Diurnal Variations of the Vostok Electric Field and Properties of Electrified PFs

The Vostok, Antarctica, electric field values are compared to numerous TRMM satellite parameters (36°N-36°S) on diurnal and seasonal timescales shown in Figure 1 in two-dimensional histograms of the electric field measurements and five selected PF parameters. Each parameter represents different PF attributes and thus the physical properties of the PFs in each panel vary from one another. Figure 1a represents the joint seasonal and diurnal variations of the relative electric field measured over the 12 years. Peaks in the electric field are present from June through October during the UTC hours of 18-23 when the American convection is most active. Smaller secondary peaks are visible from February through April at 17-21 UTC as well as in June through August at 7-10 UTC. Overall, the months of June, July, and August exhibit the largest electric fields consistently throughout the day (UTC time). This is due to the highest occurrence of electrified PFs and thunderstorms in the northern hemisphere during summer months, especially during the hours of 18-23 UTC [Orville and Spencer, 1979; Adlerman and Williams, 1996; Christian et al., 2003; Zipser et al., 2006; Blakeslee et al., 2014a]. For this case, this time also matches well with the peaks in electric field. In Figure 1b, the flash rate is represented in number of flashes per second calculated by integrating all the total lightning flashes observed by TRMM in each 1 h and 1 month bin and dividing by the total view time of the satellite and the TRMM sampled area in each hour-month bin. This is then multiplied by the total surface area in the latitude range of 36°N-36°S. This signifies the rate of lightning flashes detected by TRMM in the tropics and subtropics. The mean value of flash rate is approximately 41 flashes/second in the TRMM domain. This value is consistent with Christian et al. [2003], who document 44 flashes/seconds ±5 that occur globally.

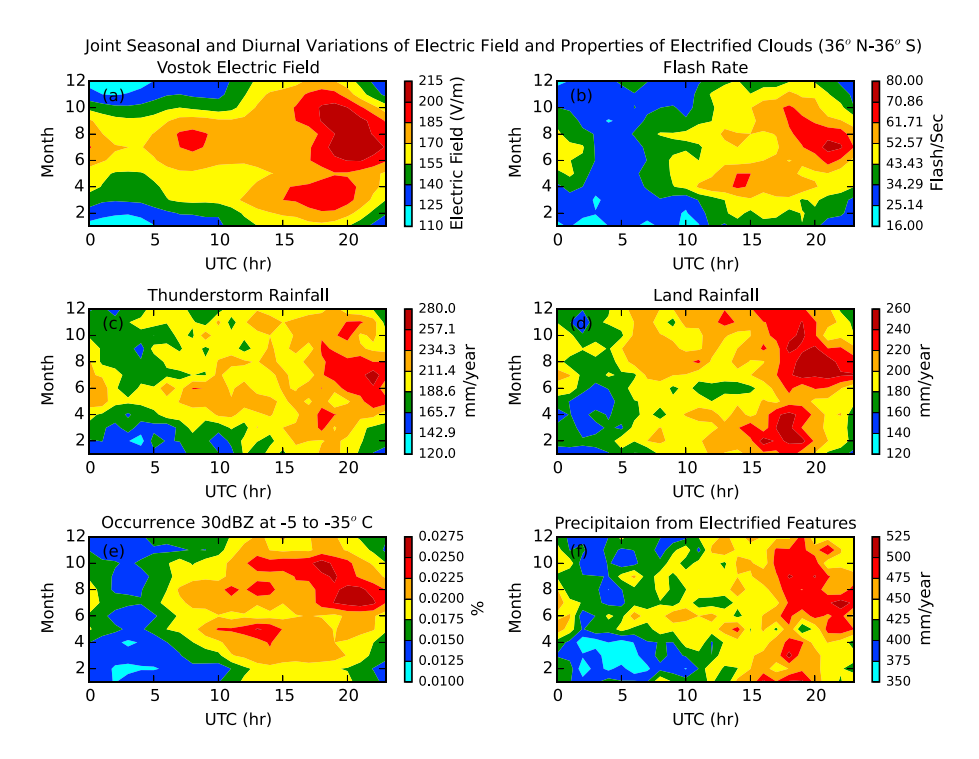


**Figure 1.** Joint diurnal and seasonal distributions of (a) the Vostok mean electric field (V/m) based on 12 years of data collected from Vostok, Antactica. Note that electric field data are averaged from two field campaigns. The absolute values shown here have large uncertainties. Here we focus on the relative diurnal-seasonal distribution pattern. (b) Mean flash rate from thunderstorms (flash/second) calculated by integrating all the total lightning strikes observed by TRMM in each 1 h and 1 month bin and dividing by the total view time of the satellite. This is then multiplied by the area of each pixel (20.35 km²) as well as the total area observed by TRMM in the 36°N–36°S orbit. (c) Precipitation from thunderstorms (mm/yr) which includes only the rainfall observed by the TRMM 2A25 algorithm from PFs with at least one flash. (d) Precipitation over land observed by the TRMM 2A25 algorithm (mm/yr). (e) Occurrence of 30 dBZ between –5 and –35°C (%) calculated as integrating the total observed volume of 30+ dBZ reflectivity in the mixed phase, divided by the total sampled pixels multiplied by the height of the mixed phase layer. (f) Precipitation from electrified features (mm/yr) defined as rainfall from the TRMM 2A25 algorithm that meets either the criteria for a thunderstorm or electrified shower cloud. All other panels are based on TRMM PF database (36°N–36°S). All values are calculated using binning of 1 h and 1 month.

Figure 1c shows the diurnal and seasonal contours of rainfall from thunderstorms alone, while Figure 1d shows the rainfall occurring only over land. Average rainfall from thunderstorms and from land based convection is very similar in quantity with both mean values between 180 and 200 mm/yr in the sampled area. Figure 1e shows the joint seasonal-diurnal variations of occurrence of 30 dBZ  $-5^{\circ}$ C to  $-35^{\circ}$ C. In the PFs these conditions are considered a proxy for the occurrence of graupel in the mixed phased region. The volume of 30 dBZ is defined as integrating all reflectivity of at least 30 dBZ and greater in the mixed phase region bounded by the temperature range of  $-5^{\circ}$ C to  $-35^{\circ}$ C. To calculate this as a percent occurrence, the total volume of 30+ dBZ is divided by the total sampled volume in the  $-5^{\circ}$ C to  $-35^{\circ}$ C prism observed by TRMM precipitation radar. This pattern is consistent for 20 and 40 dBZ (Table 1) with the calculations including total volumes of greater than or equal to the specified reflectivity thresholds. The volume of 30 dBZ found in the altitude range of  $-5^{\circ}$ C to  $-35^{\circ}$ C has been shown to have a good relationship to the flash rate in the PFs [Deierling et al., 2008; Liu et al., 2012] and could be used as one proxy for the rate of charge separation [Liu et al., 2012; Kalb et al., 2014]. Figure 1f shows the variation of rainfall from both thunderstorms and electrified shower clouds combined. This parameter approximates the rainfall from all PFs that have electrification and therefore provide a contribution to the GEC.

In many of the panels in Figure 1, similar patterns to the electric field are present. This includes maximum values seen in all panels between 18 and 22 UTC in the northern hemisphere summer months, corresponding directly to the electric field. In Figures 1d and 1f, the secondary peak in the electric field occurring between 16 and 22 UTC in February–April is present as well. This enhancement in the electric field is likely due to the local maximum in PFs over South America [Williams and Stanfill, 2002; Liu et al., 2010]. It is important to note that

**Table 1.** Linear Correlation and Standard Variation Between the Vostok Electric Field Measurements and TRMM Electrified Cloud Parameters (36°N–36°S)

Parameter	R <sup>2</sup> Value	Coefficient of Variation (%)
Electric field	_	12
Flash rate	0.67	28
Volume 20 dBZ ( $-5$ to $-35$ °C)	0.57	12
Volume 30 dBZ ( $-5$ to $-35$ °C)	0.62	19
Volume 40 dBZ ( $-5$ to $-35$ °C)	0.50	28
Ice water content 20 dBZ	0.61	12
Ice water content 30 dBZ	0.60	21
Ice water content 40 dBZ	0.52	29
Land rainfall	0.44	13
Thunderstorm rainfall	0.54	12
Global rainfall	0.19	6
Area 30 dBZ at −10°C	0.54	18
Electrified shower clouds (All)	0.10	8
Electrified precipitation features	0.48	8

the flash rate parameter (Figure 1b) does not show this secondary peak. The absence of this secondary peak is not likely to be due to the coverage of TRMM because of the small proportion of lightning outside TRMM's domain in these months. The other secondary peak in the electric field occurring during 7-10 UTC in the months of June through August is caused by the maxima of PFs over the Maritime Continent. This region peaks in electrical output between 5 and 10 UTC. Only 2.5% of the PFs coming from this region (10°S-10°N, 90°E-160°E) have lightning flashes, and 4.6% of PFs have 30 dBZ echoes

at  $-10^{\circ}\text{C}$  without lightning, indicating the importance of electrified shower clouds, especially on the eastern portion of the Maritime Continent. Further evidence of this comes from the linear correlation of 20 and 30 dBZ volume in the mixed phase region to the Vostok measured electric field (Figures 2c and 2d). This peak driven by the Maritime Continent is much more pronounced in Figure 1a than the yearly averaged diurnal variation of the GEC shown as the Carnegie Curve. This joint seasonal-diurnal perspective of the measured electric field (Figure 1a) gives a more detailed view of the GEC and how the different convection hot spots contribute to the variation in the electric field. To further represent the correlation between the electric field and electrified cloud parameters, Figure 2 illustrates the correlation of some of the tested parameters to the

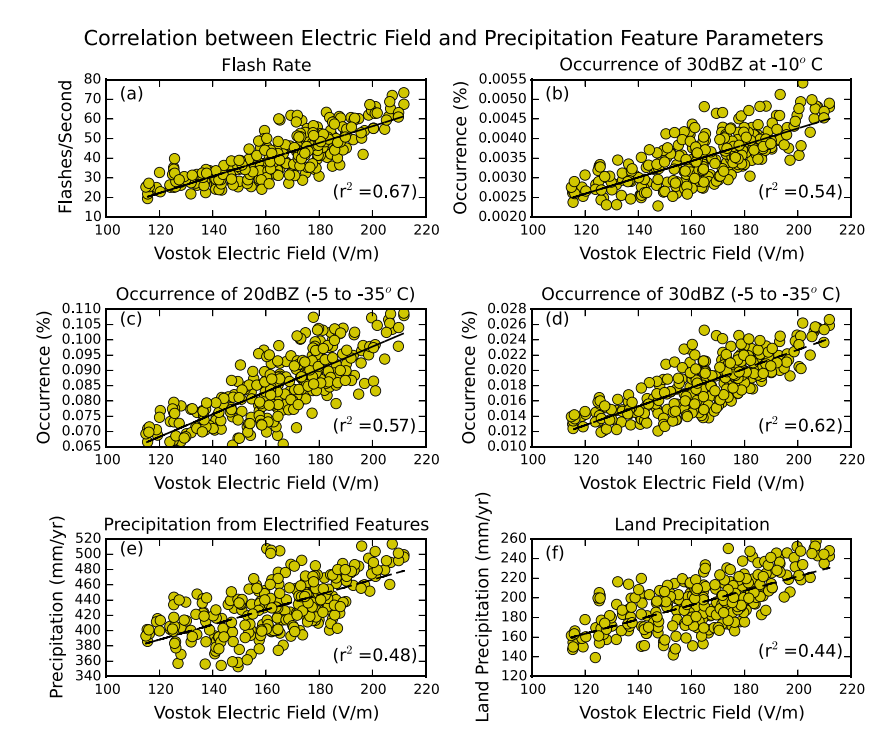


**Figure 2.** Correlation between the Vostok electric field (V/m) and (a) flash rate (flash/second). (b) Occurrence of 30 dBZ at  $-10^{\circ}$ C (%). (c) Occurrence of 20 dBZ between -5 and  $-35^{\circ}$ C (%), calculated by dividing the total volume of 30+ dBZ with the total sampled volume in the  $-5^{\circ}$ C to  $-35^{\circ}$ C prism observed by TRMM precipitation radar. (d) Occurrence of 30 dBZ between -5 and  $-35^{\circ}$ C (%). (e) Precipitation from all electrified features (mm/yr). (f) Land precipitation (mm/yr) in one monthly and one hourly bins as shown in Figure 1. Note that the absolute values of electric field have large uncertainties. Here we only focus on the correlations between the electric field with other parameters.

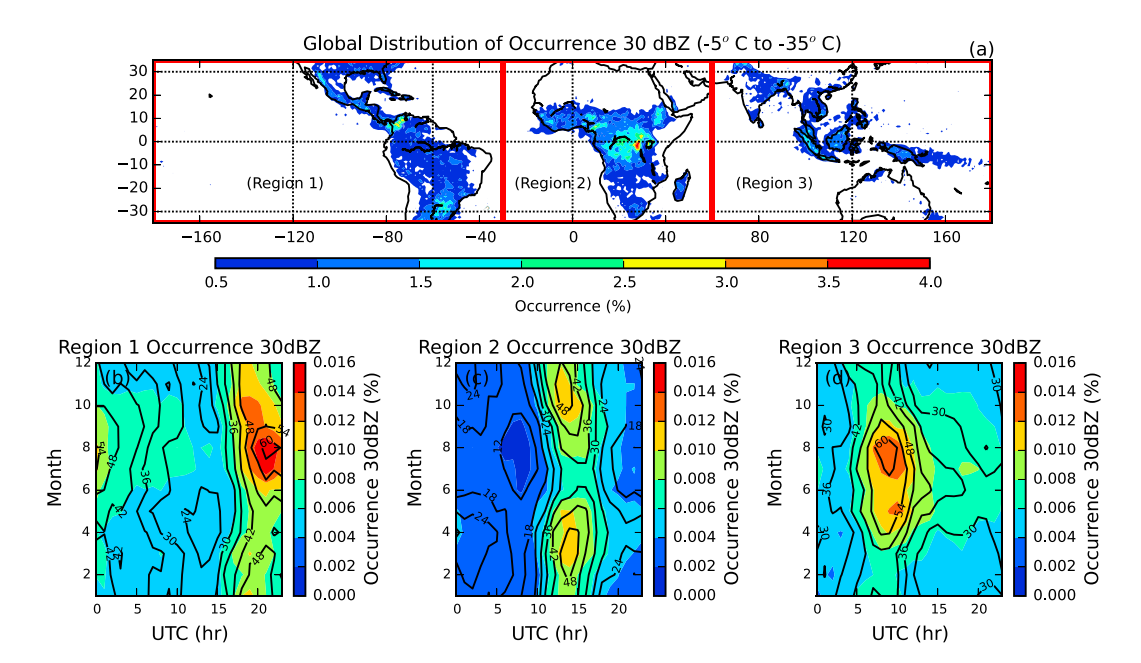


**Figure 3.** (a) Global distribution of occurrence 30 dBZ in the mixed phase region, calculated as integrating the total observed volume of 30+ dBZ reflectivity between  $-5^{\circ}$  and  $-35^{\circ}$  C, divided by the total sampled pixels observed by the TRMM precipitation radar for each  $1^{\circ} \times 1^{\circ}$  bin. (b) Joint seasonal-diurnal variation of the observed occurrence 30 dBZ in the mixed phase region observed in region 1 (-180 to -60 longitude). (c) Joint seasonal-diurnal variation of the observed occurrence 30 dBZ in the mixed phase region observed in region 2 (-60 to 30 longitude). (d) Joint seasonal-diurnal variation of the observed occurrence 30 dBZ in the mixed phase region observed in region 3 (30 to 180 longitude). All binning for Figures 3b–3d are calculated at 1 h and 1 month.

electric field in the seasonal and diurnal bins in Figure 1. In all cases, correlation coefficient values were obtained ranging from 0.44 to 0.67.

Figure 3a shows the global distribution of occurrence 30 dBZ in the mixed phase region in the TRMM domain. This clearly shows the four intense convective chimney regions (North America, South America, Central Africa, and the Maritime Continent). To demonstrate the relative contributions of the GEC from the different chimney regions, Figure 3a has been separated into regions of North and South America (-180 to -30 longitude), Central Africa (-30 to 60 longitude), and the Maritime Continent (60 to 180 longitude). Figures 3b-3d show the joint seasonal and diurnal variations of the occurrence 30 dBZ in the mixed phase region for each of the above regions. The color field represents the percent occurrence of 30 dBZ, and the contour lines represent the fractional percentage contribution from the region. Similar patterns observed in the color field can also be seen in the contour lines, with the time periods of highest occurrence of 30 dBZ for each region also dominating the global output of volume 30 dBZ for that time. Figure 3b shows the largest total occurrence of 30 dBZ with the peak occurrence in the period of June through August at 19 to 22 UTC. This corresponds well to the summertime convection maxima that occurs in North America. Figure 3c shows a bimodal distribution of peak 30 dBZ occurrence for the African region, with maxima occurring in April and October during the hours of 12 to 15 UTC. This corresponds well to the convection observed in Central Africa which propagates and is enhanced seasonally with a distinct semiannual variation within the Intertropical Convergence Zone (ITCZ) [Waliser and Gautier, 1993; Williams and Sátori, 2004]. Figure 3d, relevant to the Maritime Continent, shows the maximum 30 dBZ occurrence at 5 to 10 UTC in the months of May through September. This is the peak convective time period for the Maritime Continent consistent with the classical analysis of the GEC [Whipple, 1929].

In addition to the parameters shown in Figures 1 and 2, we have also tested the joint seasonal and diurnal correlations of the electric field to other TRMM parameters that are relevant to the ice-based charge separation processes. These include volume of 20 and 40 dBZ radar echoes, ice water content in the mixed phase region, area of 30 dBZ at  $-10^{\circ}$ C, and rainfall from electrified shower clouds (figures not shown). The correlations and variation coefficients are listed in Table 1. All tested parameters show clear positive relationships



with the electric field values, with the flash rate parameter alone being able to account for approximately two thirds of the joint seasonal and diurnal variations seen in the electric field based on the  $r^2$  statistic. Flash rate shows the prevalence of lightning flashes occurring at all times of the year. Although flash rate had the best linear correlation, it also had a much higher coefficient of variation (COV) (28%) than the electric field (12%). This is consistent with earlier studies showing a larger amplitude of lightning's diurnal variation than the "Carnegie curve" [Williams and Heckman, 1993; Mach et al., 2011; Blakeslee et al., 2014a]. In the past, when comparing these cloud parameters to the yearly averaged diurnal curves of the electric field, claims have been made that lightning flash rate might not be the main driver of the DC global circuit [Wilson, 1920; Williams and Heckman, 1993].

Another good correlation to the electric field is from the occurrence of 30 dBZ in the altitude range of -5 to -35°C (Figures 1e and 2d). The occurrence of 30 dBZ in the mixed phased region theoretically includes the region and conditions of the atmosphere best suited for charge separation to occur [Takahashi, 1978]. Large enough ice particles represented by the 30 dBZ radar reflectivity are present in the cloud. These graupel particles, combined with the presence of supercooled liquid water, collide with smaller ice particles to increase the electrical charge separation. The occurrence of 20 dBZ and 30 dBZ in the mixed phase region has a more consistent amplitude agreement with the electric field with COV being 12% and 19%, respectively. Compared to the electric field (12% variation), the occurrence of 20 dBZ and 30 dBZ in the mixed phased region has a much closer amplitude agreement than the flash rate (28%). This is probably due to the inclusion of contribution from PFs without lightning that are left out in the flash rate variable, which have a relatively small diurnal amplitude variation compared to the flash rate (8% compared to 28%) [Liu et al., 2010].

These joint diurnal and seasonal results support the flash rate and thunderstorm variables being directly correlated to the GEC at both the diurnal and seasonal timescales. These results further validate the storm theory of the GEC that electrified clouds, including thunderstorms and electrified shower clouds, act as the battery of the GEC that produces a current within the global circuit that can be detected in surface electric field measurements.

#### 3.2. Variations of the Vostok Electric Field and Properties of Electrified PFs Corresponding to ENSO

The ENSO variation [Philander, 1989; Allan et al., 1996] occurs at relatively long timespans (2–7 years) and likely has a significant impact on the distribution and occurrence of electrified clouds [Goodman et al., 2000; Chronis et al., 2008; Chen et al., 2014; Dowdy, 2016]. Furthermore, ENSO events, having two distinct and opposite phases, allowing for direct and clear comparisons to be made between the two phases (El Niño and La Niña). It is well known that the shifting Walker circulation due to the ENSO variation causes the trade winds to switch directions and bring heavier rains and more thunderstorms to South America and the Maritime Continent [Williams and Sátori, 2004]. Much previous work has looked into the comparison of rainfall and lightning variation on the ENSO timescale both regionally and globally. Over the convective chimney regions (Amazon, Nile, and Congo), an increased river discharge can be observed during La Niña periods [Hirst and Hastenrath, 1983; Richey et al., 1989; Eltahir, 1996; Amarasekera et al., 1997]. This provides evidence that these tropical continental regions receive statistically significant more rainfall in ENSO's cool period. An analysis of the Southeastern United States Gulf Coast region using the TRMM LIS as well as the National Lightning Detection Network shows that the latter region receives a considerable increase (nearly 200%) in lightning hours in the El Niño winter period (December-February) of 1997 in comparison to the following year [Goodman et al., 2000]. Previous studies in Brazil have tied thunderstorm occurrence to ocean variability [Pinto et al., 2013]. Results show that more thunderstorms occur in Brazil during the La Niña phase of ENSO. The total number of lightning flashes are enhanced in Southeast Asia by 12% in El Niño years and suppressed by 5% in La Niña years [Kumar and Kamra, 2012]. A recent study in Southern China shows that the region receives higher than average rainfall during winter and spring in El Niño periods [Chen et al., 2014]. The western region of the Maritime Continent shows increased lightning as well as decreased rainfall in El Niño periods [Hamid et al., 2001; Chronis et al., 2008; Satori et al., 2009]. Further detailed worked into the temporal variation of lightning caused by ENSO variability shows seasonal variation as well, with many regions of the world showing correlations between the season and ENSO index [Dowdy, 2016].

The natural interannual variability of electrified cloud properties caused by ENSO can be compared to the variation seen in the GEC during the same time periods. For this reason, using the natural ENSO climate variation

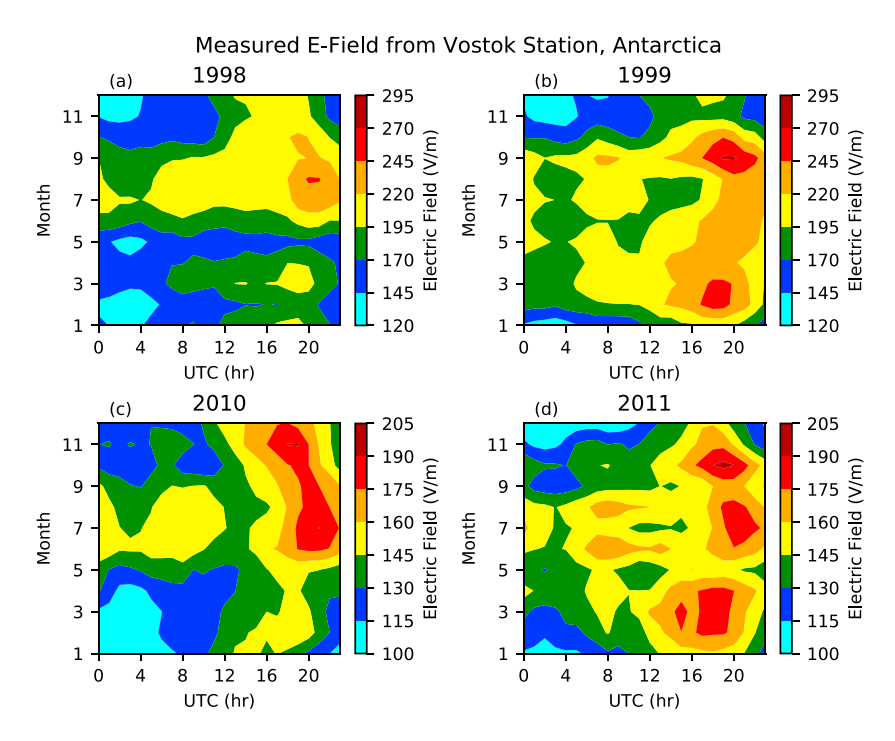


**Figure 4.** Diurnal and seasonal histograms showing the difference in the Vostok electric field (V/m) during (a and c) El Niño years and (b and d) La Niña years. All values are calculated using binning of 1 h and 1 month bins. Note that the different color scales are used in years for two field campaigns. The absolute values in these panels have large uncertainties. Here we focus only on the diurnal seasonal variation patterns.

can be very useful in understanding if the interannual variability of the GEC is also driven by the distribution of global electrified clouds. This comprehensive look at multiple timescales (diurnal, seasonal, and interannual) with quasi-global coverage gives a direct comparison of the similarities and differences between the variation of electrified cloud parameters and the measured electric field.

Figure 4 shows the difference in Vostok electric field values during El Niño and La Niña time periods. As previously stated, El Niño was defined as any time period with an ONI index of greater than +0.5 and La Niña periods were defined as any periods with the ONI of less than -0.5. The early half of 1998 and 2010 are considered to be months dominated by El Niño conditions, while 1999 and 2011 are considered to be strong La Niña years. Figure 4 shows large seasonal differences in the electric field values throughout the year. This variation is likely due to the regional changes of PFs caused by the ENSO warming or cooling. The most significant difference in fair weather electric field values occurs between 16 and 24 UTC during the months of January through April, which also corresponds well to the months with the largest difference in ONI values. A significant increase in the electric field is observed over this time period in La Niña years. This is where the largest observable difference in electric field appears between the El Niño and La Niña years.

The heavier rainfall and increased thunderstorm activity in the late afternoon hours over South America including the Amazon and Argentina regions corroborate well with the increased electric field observed during January–April 16–24 UTC in Figure 4. The continent of South America dominates the global contribution to the fair weather electric field during the timespan of 16–24 UTC in the Austral summer months [*Liu et al.*, 2010; *Blakeslee et al.*, 2014a]. The increase in the electric field during the time dominated by South America under the La Niña phase (in two episodes) implies that the ENSO variation has a strong impact on the global fair weather electric field.

Figure 5 shows the joint seasonal-diurnal variations of the electric field as well as volume of 30 dBZ between  $-5^{\circ}$ C and  $-35^{\circ}$ C, total rainfall over land as seen by TRMM ( $36^{\circ}$ N $-36^{\circ}$ S), and the flash rate in the El Niño and La Niña time periods. For each month, the data from the two strongest ENSO periods are included for both El Niño and La Niña periods. It is important to note for the electrified cloud parameters, only 1 year of La Niña occurred with an ONI value of less than -0.5 only in the months of May and June. This possibly explains the poor correlation with TRMM electrified cloud parameters and increased values observed in those months.

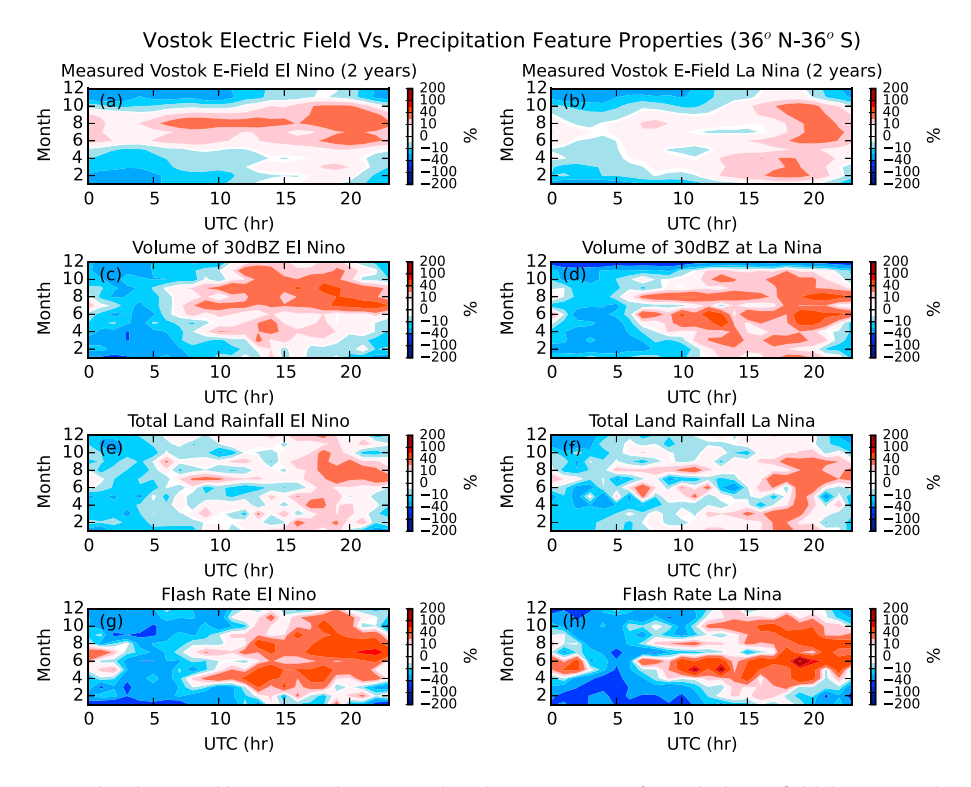


**Figure 5.** Diurnal and seasonal histograms showing (a) the relative variations of Vostok electric field during two El Niño periods, (b) the relative variations of Vostok electric field during two La Niña periods, and (c) the volume 30 dBZ occurrence between -5 and  $-35^{\circ}$ C during the same El Niño periods, calculated as integrating the total observed volume of 30+ dBZ reflectivity divided by the total sampled pixels observed by TRMM for each bin. (d) The volume 30 dBZ occurrence between -5 and  $-35^{\circ}$ C during the same La Niña periods and (e) the total land rainfall during El Niño years, calculated as rainfall as seen by the TRMM 2A25 algorithm over land. (f) The total rainfall from La Niña years and (g) the flash rate from El Niño years, calculated by integrating all the total lightning strikes observed by TRMM in each 1 h and 1 month bin and dividing by the total view time of the satellite. This is then multiplied by the area of each pixel (20.35 km²) as well as the total area observed by TRMM in the  $36^{\circ}$ N- $36^{\circ}$ S orbit. (h) The flash rate from La Niña years. The ENSO time periods were determined by choosing the two largest Oceanic Nino Index (ONI) values for each month in El Niño years (1998–2004 and 2007–2011) and the two smallest ONI values for each month in La Niña years (1998–2004 and 2007–2011). All values are represented as a variation from the variable's yearly mean value. All values are calculated using binning of 1 h and 1 month.

With the exception of those poorly sampled months, many of the patterns that are visible in the electric field measurements are also shown with similar patterns in the cloud parameters. More data are needed, especially in La Niña years to ultimately verify this correlation. In the El Niño periods the values of 30 dBZ volume in the mixed phase region, total rainfall over land, and the flash rate (Figures 5c, 5e, and 5g) maximize in the hours of 18-23 UTC in the months of June through August, which corresponds to the high electric field values (Figure 5a). Also, it is important to note the suppression of the electric field (Figure 5a), as well as total land rainfall (Figure 5e) and volume of 30 dBZ (Figure 5c) at 16-24 UTC during January through April. For the La Niña periods (Figures 5b, 5d, and 5f), a strong enhancement throughout the entire South America afternoon (16-20 UTC) is shown in the electric field from February to April. Although slightly weaker, this same trend can be found in the corresponding PF parameters in Figures 5d and 5f as well. The TRMM flash rate (Figures 5g and 5h) does not observe any La Niña enhancement in the time period of 16-24 UTC in the Austral summer months. Very little visable difference in the Austral summer months between 16 and 24 UTC is seen in the flash rate between the ENSO phases. This is likely due to electrified shower clouds having a large electrical contribution to this time period mainly coming from South America and the Maritime Continent that is not seen in the flash rate [Liu et al., 2010]. This could explain the better ENSO correlation seen in the volume 30 dBZ in the mixed phase region and the land rainfall variables, which include shower clouds as well as thunderstorms. The color scale of Figure 5 indicates the variation in amplitude of the electrified cloud parameters compared to the electric field on the ENSO timescale. The electric field (Figures 5a and 5b) has a relatively small COV, with the overall variation of the data ranging from approximately -40% to 40% from the mean. Global land rainfall as seen by TRMM

**Table 2.** Linear Correlation Coefficient ( $R^2$ ) and Standard Variation (COV) Between the Vostok Electric Field Measurements and TRMM Electrified Cloud Parameters (36°N–36°S) During Each Phase of the ENSO Cycle

Parameter:	El Niño (R <sup>2</sup> )	La Niña (R <sup>2</sup> )	Coefficient of Variation el Nino (%)	Coefficient of Variation la Nina (%)
Electric field	-	_	12	12
Volume 20 dBZ ( $-5$ to $-35$ °C)	0.45	0.37	13	14
Volume 30 dBZ ( $-5$ to $-35$ °C)	0.48	0.40	20	20
Volume 40 dBZ ( $-5$ to $-35$ °C)	0.32	0.28	30	34
Ice water content 20 dBZ	0.46	0.39	13	13
Ice water content 30 dBZ	0.45	0.37	23	23
Ice water content 40 dBZ	0.34	0.29	31	34
Land rainfall	0.22	0.32	14	16
Thunderstorm rainfall	0.23	0.20	14	16
Electrified precipitation features	0.31	0.18	10	11
Flash Rate	0.36	0.39	31	35

(Figures 5e and 5f) has a very similar coefficient of variation of the data, also ranging from approximately -40% to 40% from the mean. The volume 30 dBZ parameter (Figures 5c and 5d) has an amplitude of roughly double that of the electric field on these timescales, and the flash rate (Figures 5g and 5h) has an even stronger amplitude ranging from approximately -180% to 180% from the mean. Some of the strong variation seen in the flash rate variable can be attributed to the lack of samples in the La Niña months of May and June, but it is clear that the flash rate has a much larger UT diurnal amplitude than that of the electric field. This is reminiscent of Williams and Heckman [1993] and also suggests a decoupling of the DC and AC global circuits. Of these tested electrified cloud parameters, flash rate has a joint seasonal and diurnal correlation to the electric field on the ENSO timescale with  $r^2$  values of 0.36 and 0.39 for El Niño and La Niña, respectively, at 99% level of confidence. Despite having one of the better correlations tested, flash rate also had one of the highest COV of all the tested variables. Table 2 summarizes the correlation of all tested PF parameters with the Vostok electric field during both El Niño and La Niña periods. All parameters have a highly significant correlation with the electric field with P values much less than 0.01. The correlation coefficient ranges from 0.18 to 0.48 for the parameters, with the best parameter to see the difference in the ENSO years appearing to be volume 30 dBZ (-5 to -35°C). Again, the spread of the flash rate variable was observed to be much larger than the electric field with a COV being 31% in the El Niño periods and 35% in the La Niña periods.

To possibly demonstrate the source of the enhancement of the PF parameters during the critical time period of 16–24 UTC and January through April, Figure 6 shows the distribution of the observed volume of 30 dBZ in the mixed phase region during six selected years (three strongest El Niño and three strongest La Niña years for each month were chosen) and differences between in El Niño years and La Niña years in the time period of 16-24 UTC from January through April. Figure 6a shows the 6 year total of 30 dBZ volume (km<sup>3</sup>) in each  $10^{\circ} \times 10^{\circ}$  grid box. As stated previously, volume 30 dBZ in the mixed phase region can possibly be used as a proxy for charge separation in a cloud. Solely using TRMM data such as volume 30 dBZ allows for more years to be analyzed, due to the longer running and more complete data set in comparison to the Vostok electric field data. This addition of 2 years makes the analysis between the two ENSO phases more robust. Selecting this important 4 month period of January-April allows for three complete El Niño periods to be compared to three complete La Niña periods. As mentioned before, South America dominates the total volume of 30 dBZ in the mixed phase region during this time. Central Africa and the maritime continent are also seen to have a significant amount of volume 30 dBZ between  $-5^{\circ}$ C and  $-35^{\circ}$ C. Figure 6b shows the difference in the volume (km<sup>3</sup>) in the mixed phase region between El Niño and La Niña years. The warm colors (red) represent the areas where El Niño had a higher volume of 3 dBZ, and the cool colors (blue) represent where La Niña dominated the amount of volume 30 dBZ. Regional differences are clearly visible, which is expected due to the precipitation shifts caused by the ENSO periods. The regions of most importance are the locations that show the largest amount of volume 30 dBZ during this time such as South America, Central Africa, and the Maritime Continent (Figure 6a). When observing the ENSO difference in this volume, it is clear that South America shows a much larger volume 30 dBZ in La Niña years, especially over the Amazon region (Figure 6b). The eastern portion of the Maritime Continent region is also dominated by the La Niña phase of the ENSO cycle with 30 dBZ volume as much as  $1.5 \times 10^6 \ km^3$  more than in El Niño time periods, during the six

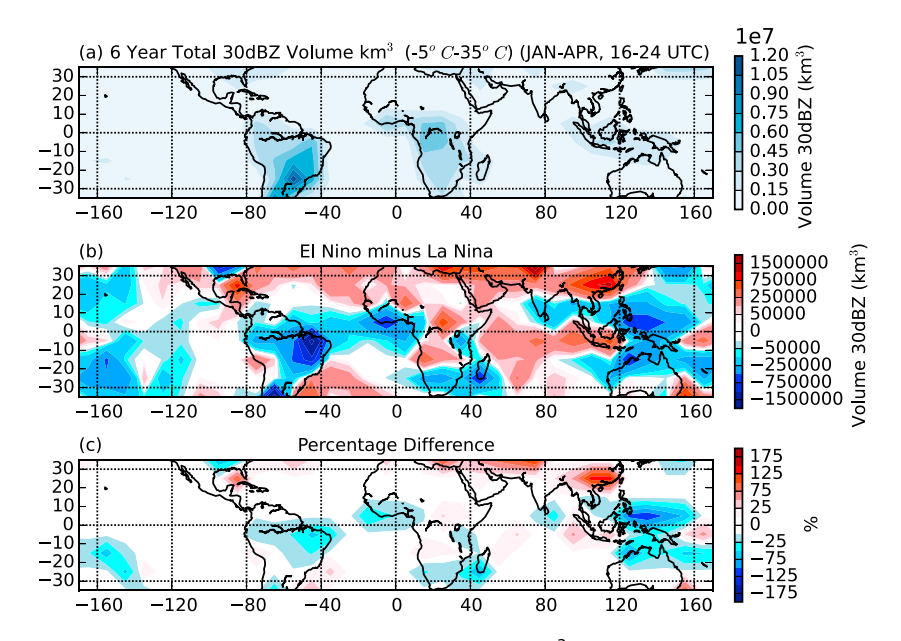


**Figure 6.** Difference between the geo-distribution of volume 30 dBZ (km $^3$ ) in El Niño periods and in La Niña phases during the time period of January–April (16–24 UTC). (a) The 6 year total volume 30 dBZ received in each 10° × 10° grid box. (b) The difference of volume 30 dBZ (km $^3$ ) in El Niño years minus La Niña years in each 10° x 10° grid box. The warm colors represent where El Niño received a larger amount of volume 30 dBZ (km $^3$ ), and the cool colors represent where La Niña received more volume 30 dBZ (km $^3$ ). (c) The percentage difference of volume 30 dBZ (km $^3$ ) from the mean value for each 10° x 10° grid box and is defined as ((El Niño – La Niña)/((El Niño + La Niña)/2)) \* 100.

sampled years. Central Africa is mixed with roughly half of the region (east central Africa) dominated by El Niño years and the other half (Gulf of Guinea) dominated by La Niña years. These results are consistent with Dowdy [2016]. Figure 6c shows the percent difference from the mean value in each  $10^{\circ} \times 10^{\circ}$  grid box. Again, the same pattern is visible with the highest percent differences of significance occurring over South America and the eastern half of the Maritime Continent.

Figure 7 shows the same geo-distribution and ENSO differences as seen in Figure 6, except with the flash-count variable. The flash rate variable was chosen to compare to the global distribution of volume of 30 dBZ in the mixed phase region. This can provide valuable information about the types of systems that occur over different regions. Figure 7a has nearly the same geo-locational distribution as shown in Figure 6a with the exception of the noticeable lack of lightning in the eastern portion of the Maritime Continent. This is explained by the PFs without flashes having 30 dBZ echoes in the mixed phase region that occur over this region, which are primarily electrified shower clouds and thus do not produce lightning. A hot spot in lightning can be seen over Argentina, with as many as 17,500 flashes occurring over a relatively small area during the 6 year period shown by TRMM. Lightning is almost solely dominated by South America and Central Africa over this time period. Figures 7b and 7c show that of these two areas, South America has a much higher total flashcount and percent difference from the mean in La Niña years than in El Niño years. As many as 3000 more lightning strikes/year/10° × 10° grid box are seen in the Amazon in La Niña years than in El Niño years during the four sampled months. Central Africa is roughly equally split between El Niño and La Niña dominance, with nether taking precedence over the other. For this reason, South America during the time period of January–April 16–24 UTC dominates the global influence of lightning on the GEC.

The results seen in Figures 6 and 7 correlate very well with the electric field shown in Figure 4 where the time period of January–April 16–24 UTC is enhanced in La Niña years. This same trend is visible in the two separate data sets and provides strong evidence that the two are in fact correlated.

## 4. Discussion

# 4.1. Long-Standing Discrepancy Between Lightning and the DC Global Circuit

As shown by the Carnegie Curve, the maxima in the GEC is observed at approximately 19–20 UTC. This is inconsistent with the maxima in global lightning activity driven by Africa which occurs at approximately 15

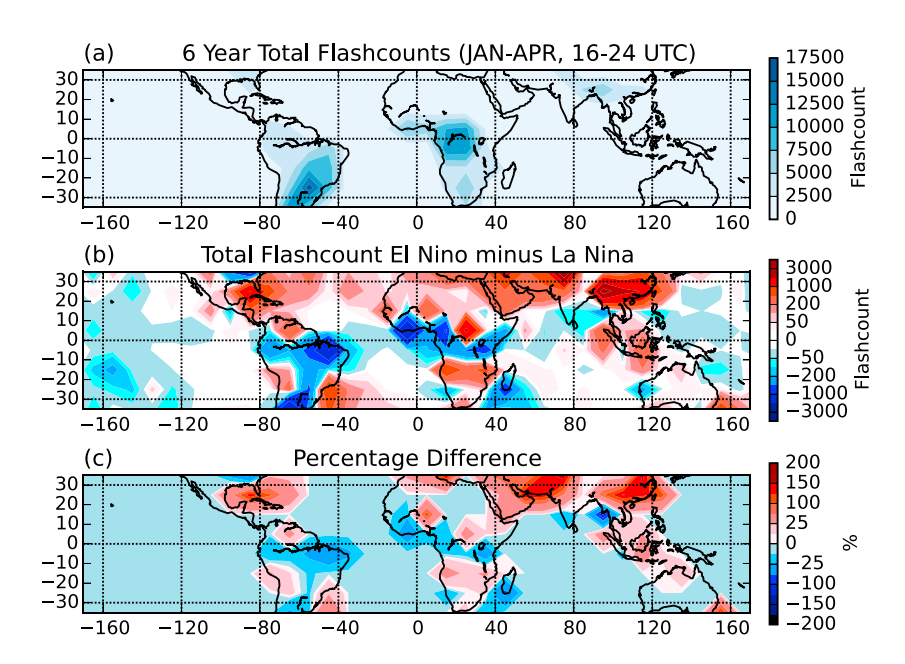


**Figure 7.** Subtraction of the geo-distribution of flashcount during El Niño and La Niña phases during the time period of January–April (16–24 UTC). (a) The 6 year total flashcount received in each 10° x 0° grid box. (b) The difference in the flashcount in El Niño years minus La Niña years in each 10° x 10° grid box. The warm colors represent where El Niño received a larger number of lightning flashes, and the cool colors represent where La Niña received more lightning flashes. (c) The percentage difference of flashcount from the mean value for each 10° x 10° grid box and is defined as ((El Niño – La Niña)/ ((El Niño + La Niña)/2)) \* 100.

UTC [Christian et al., 2003; Blakeslee et al., 2014a]. Over the last several decades, it has been increasingly recognized that electrified shower clouds are extremely important in understanding the variation in the DC electric circuit [Williams and Heckman, 1993; Williams, 2009; Liu et al., 2010; Mach et al., 2011].

Results from this manuscript provide further evidence into this claim that electrified shower clouds play a large role in the DC circuit. Figures 3 and 6 show the relative dominance in the occurrence of 30 dBZ volume in the mixed phase region of the Americas over Africa. This indicates that although lightning is more prevalent in Africa (Figures 1b and 7), electrified shower clouds are more common in the Americas and the Maritime Continent than over Africa. Figure 3 indicates a relatively larger contribution to the DC electric circuit coming from the Americas than Africa, represented by the 30 dBZ volume. As stated previously, this parameter is a very good indicator of charge separation and can be representative of both thunderstorms and electrified shower clouds. This could imply that although Africa exhibits much more lightning than the Americas, a larger total charge separation in moist convection occurs in the 20 UTC time frame, driven by the Americas. This observed maxima of volume 30 dBZ and land rainfall (both of which include contributions from electrified shower clouds) in the Americas at approximately 20 UTC matches much better to the maxima in the electric field than that of lightning flash rate alone. This could provide some clarity and explanation for the longstanding puzzlement about the relationship between lightning and the DC global circuit and provides evidence for the importance of volume of 30 dBZ in the mixed phase region globally to the DC circuit.

# 4.2. Variation of the Global Electric Circuit Corresponding to ENSO

It is well known that the warming and cooling anomaly of the eastern Pacific Ocean influences rainfall and convection around the tropics and subtropics [Ropelewski and Halpert, 1987]. Here the variation of electrified PF parameters and the GEC due to the ENSO variability have been examined at the seasonal and diurnal scales. In all reviewed cases, clear ENSO relationships were observed in the joint seasonal and diurnal variations of the electric field. In the important time period of January through April during 16–24 UTC, La Niña periods have an enhanced electric field, while El Niño periods exhibit a suppressed electric field. The enhancement of the electric field during the Austral summer 16–24 UTC in La Niña periods is correlated well with the increased rainfall and graupel at mixed phased region observed in South America, which dominates



the global convection fraction during this time. This suggests that ENSO has stronger influences on South America than on other regions during this season. This also confirms the different seasonal variations of the correlations between the lightning and ENSO index over various regions presented by *Dowdy* [2016]. However, Dowdy's result suggests a very small percentage anomaly (less than 25%) of lightning over south America in the December-January-February and March-April-May [*Dowdy*, 2016, Figures 4a and 4b]. The main reason for this discrepancy is that most regions with high correlations between flash rate and ENSO index and large percentage flash rate anomaly in *Dowdy* [2016], such as the east Pacific ITCZ and winter time land, have low flash rates. Although there is a large fractional increase or decrease of flash rate over those regions, their contributions to the total variation of global lightning is not important. To mitigate the GEC, it is more important to understand the variations over the regions where the electrified systems are more active, such as South America between January and April. Further study of how the systems over the lightning-active regions vary under different ENSO phases is warranted. Nevertheless, in this study, the corroboration of the two separate data sets (TRMM and Vostok electric field) at the diurnal, seasonal, and ENSO timescales provides solid evidence that the global electrified shower clouds are tightly related to the fair weather electric field and the GEC.

# 5. Summary

Using electric field measurements over the course of 12 years from Vostok Station, Antarctica, and 16+ years of TRMM PF observations of precipitation systems in the tropics and subtropics, the joint seasonal and diurnal variations of electric field, and selected properties of precipitation systems are compared. Influences on the GEC are also demonstrated in the different seasonal-diurnal variation patterns from electric field and properties of precipitation systems. The major findings include the following:

- All tested PF parameters show a positive correlation to the measured electric field at joint seasonal and diurnal timescales. Flash rate and the occurrence of 30 dBZ in the range of -5 to -35°C have very good correlations, but it is difficult to give the physical basis for which parameters are best for comparison with the electric field. For example, land rainfall tends to do the best job at picking up the "hot spots" in the electric field. Conversely, flash rate does not correlate as well to the secondary hot spots in the electric field occurring between 16 and 22 UTC in February–April and June–August 5–10 UTC but does have the overall best linear correlation. No direct, solid conclusions can be made as to which single parameter is considered the "best."
- The diurnal and seasonal variabilities of the electric field are shown at the ENSO timescale. Major differences are visible between the El Niño electric field and the La Niña electric field, especially during the Austral summer months. The time from 16 to 22 UTC and January through April has an enhanced electric field in the La Niña years. This gives supporting evidence that natural variation in the Earth's climate can also be observed in the measured electric field.
- Similar El Niño and La Niña differences at the joint seasonal and diurnal timescales are also observed in the parameters of precipitation systems, e.g., volume of 30 dBZ in the mixed phase region, land rainfall, etc. This provides even further evidence that precipitation systems around the globe have a direct connection to the GEC.

This heightened electric field and global PF data set gives us a better ability to correlate the electric field to various global cloud parameters. However, improvements in our understanding of the cloud microphysical processes are still needed in order to understand the true role of global electrified clouds in the GEC.

A larger set of electric field measurements is vital to determine more of the interannual variability of the electric field, especially when comparing to ENSO and other longer-term cycles. The 12 years of running data from the Vostok station are a good start but still provide only limited data that allow for preliminary conclusions about the correlation of the electric field at interannual timescales. Having a larger data set of electric field measurements at additional stations, such as at the Arctic or in Greenland, would provide a clearer picture of the year-to-year pattern of the electrified cloud parameter variation that influences the electric field with the addition of data in the northern hemisphere.

Furthermore, TRMM only observes the tropics of the Earth (36°N–36°S). The TRMM data set misses the northern hemisphere summer thunderstorms that occur in the mid-to-high latitudes. For example, the summer thunderstorms in the Great Plains of the United States, in Russia, and in Europe are completely



missing in the TRMM correlation. Theoretically, if these missing PFs were to be included in the data analysis, the result would give us clearer results as to the true total contribution from electrified precipitation systems to the electric field. The absence of these high-latitude PFs could also account for the differences shown in June-July-August in Figures 3 and 4. The results, however, suggest that tropical convection plays a major role in the GEC and that changes seen in South America are well correlated to the changes in the measured electric field, despite TRMM not observing the higher latitudes. The Global Precipitation Mission (GPM) satellite was launched in 2014 and currently has over 2 years of data. This satellite mission extends the scope of sampling from tropics and subtropics (36°N-36°S) to mid-high latitudes (65°N-65°S). This includes the higher-latitude precipitation systems that are missing in the TRMM data set with the exception of flash rate. Other newly launched instruments include the Lightning Imaging Sensor onboard the International Space Station (ISS) [Blakeslee et al., 2014b], as well as the Lightning Mapper onboard the Geostationary Operational Environmental Satellite R-Series (GOES-R) [Goodman et al., 2013]. This ISS LIS will extend the coverage of lightning observations to approximately 54°N-54°S. The GOES-R satellite, which is geostationary over the Americas, will provide a continuous observation of lightning in the American convective chimney. With the use of the new GPM data set, alongside the ISS-LIS and the GOES-R, we can get a better representation of electrified cloud parameters around the globe. This would enhance our understanding of the true electrified cloud properties and their total overall contribution to the GEC.

#### Acknowledgments

We would like to thank the generous contributions and ideas from Farle Williams and two other anonymous reviewers that greatly improved the quality of this work. This study was supported by National Science Foundation-1519006 and NASA PMM science NNXAD76G. Thanks to Erich Stocker and the Precipitation Processing System (PPS) team at NASA Goddard Space Flight Center, Greenbelt, MD, for TRMM data processing assistance. This TRMM data can be downloaded from http://atmos.tamucc. edu/trmm/data/. The Vostok electric field data were collected by specialists of the Russian Antarctic program under a collaborative Russian-Australian program and downloaded from the Australian Antarctic Data Center (http:// data.aad.gov/au). We thank Greg Lucas for processing the raw data and converting the signals into electric field values. The Burns et al., 2012 data were downloaded at http://data.aad.gov.au/ metadata/records/AAS 974 Vostok 2006to2011 20min. The ENSO index is downloaded from http://www.cpc. noaa.gov/products/analysis monitoring/ensostuff/ensoyears.shtml.

#### References

- Adlerman, E. J., and E. R. Williams (1996), Seasonal variation of the global electrical circuit, J. Geophys. Res., 101, 29,679, doi:10.1029/ 96JD01547.
- Allan, R. J., J. Lindesay, and D. Parker (1996), El Niño Southern Oscillation and Climatic Variability, 402 pp., CSIRO Publishing, Collingwood, Australia.
- Amarasekera, K. N., R. F. Lee, E. R. Williams, and E. A. B. Eltahir (1997), ENSO and the natural variability in the flow of tropical rivers, J. Hydrol., 200, 24-39,
- Blakeslee, R. J., D. M. Mach, M. G. Bateman, and J. C. Bailey (2014a), Seasonal variations in the lightning diurnal cycle and implications for the global electric circuit. Atmos. Res., 135–136, 228–243, doi:10.1016/j.atmosres.2012.09.023.
- Blakeslee, R. J., et al. (2014b), Lightning Imaging Sensor (LIS) for the International Space Station (ISS): Mission description and science goals. Burns, G. B., A. V. Frank-Kamenetsky, O. A. Troshichev, E. A. Bering, and B. D. Reddell (2005), Interannual consistency of bi-monthly differences in diurnal variations of the ground-level, vertical electric field, J. Geophys. Res., 110, D10106, doi:10.1029/2004JD005469.
- Burns, G. B., B. A. Tinsley, A. V. Frank-Kamenetsky, O. A. Troshichev, W. J. R. French, and A. R. Klekociuk (2012), Monthly diurnal global atmospheric circuit estimates derived from Vostok electric field measurements adjusted for local meteorological and solar wind influences, J. Atmos. Sci., 69(6), 2061-2082, doi:10.1175/JAS-D-11-0212.1.
- Burns, G. B., A. V. Frank-Kamenetsky, B. A. Tinsley, W. J. R. French, P. Grigioni, G. Camporeale, and E. A. Bering (2017), Atmospheric global circuit variations from Vostok and Concordia electric field measurements, J. Atmos. Sci., 74(3), 783-800, doi:10.1175/JAS-D-16-
- Carey, L. D., and S. A. Rutledge (1996), A multiparameter radar case study of the microphysical and kinematic evolution of a lightning producing storm, Meteorol. Atmos. Phys., 59(1-2), 33-64, doi:10.1007/BF01032000.
- Chen, J., Z. Wen, and R. Wu (2014), Interdecadal changes in the relationship between Southern China winter-spring precipitation and ENSO, Clim. Dynam., 1327-1338, doi:10.1007/s00382-013-1947-x.
- Christian, H. J., et al. (2003), Global frequency and distribution of lightning as observed from space by the Optical Transient Detector, J. Geophys. Res., 108(D1), 4005, doi:10.1029/2002JD002347.
- Chronis, T. G., S. J. Goodman, D. Cecil, D. Buechler, F. J. Robertson, J. Pittman, and R. J. Blakeslee (2008), Global lightning activity from the ENSO perspective, Geophys. Res. Lett., 35, L19804, doi:10.1029/2008GL034321.
- Corney, R. C., G. B. Burns, K. Michael, A. V. Frank-Kamenetsky, O. A. Troshichev, E. A. Bering, V. O. Papitashvili, A. M. Breed, and M. L. Duldig (2003), The influence of polar-cap convection on the geoelectric field at Vostok, Antarctica, J. Atmos. Sol. Terr. Phys., 65(3), 345-354, doi:10.1016/S1364-6826(02)00225-0.
- Deierling, W., W. A. Petersen, J. Latham, S. Ellis, and H. J. Christian (2008), The relationship between lightning activity and ice fluxes in thunderstorms, J. Geophys. Res., 113, D15210, doi:10.1029/2007JD009700.
- Dowdy, A. J. (2016), Seasonal forecasting of lightning and thunderstorm activity in tropical and temperate regions of the world, Nat. Publ. Gr., (May 2015), 1-10, doi:10.1038/srep20874.
- Eltahir, E. (1996), El Nifio and the natural variability in the flow of the Nile River Ocean, and the flow of water in the Nile River. The analysis, Water Resour. Res., 32, 131-137.
- Frank-Kamenetsky, A. V., G. B. Burns, O. A. Troshichev, V. O. Papitashvili, E. A. Bering, and W. J. R. French (1999), The geoelectric field at Vostok, Antarctica: Its relation to the interplanetary magnetic field and the cross polar cap potential difference, J. Atmos. Sol. Terr. Phys., 61(18), 1347-1356, doi:10.1016/S1364-6826(99)00089-9.
- Goodman, S. J., D. E. Beuchler, K. Knupp, K. Driscoll, and E. W. McCaul Jr. (2000), The 1997–98 El Niño event and related wintertime lightning variations, Geophys. Res. Lett., 27, 541-544.
- Goodman, S. J., et al. (2013), The GOES-R geostationary lightning mapper (GLM), Atmos. Res., 125, 34-49.
- Hamid, E. Y., Z. I. Kawasaki, and R. Mardiana (2001), Impact of the 1997–98 El Niño event on lightning activity over Indonesia, Geophys. Res. Lett., 28, 147-150, doi:10.1029/2000GL011374.
- Harrison, R. G., M. Joshi, and K. Pascoe (2011), Inferring convective responses to El Niño with atmospheric electricity measurements at Shetland, Environ. Res. Lett., 6(4), 44028, doi:10.1088/1748-9326/6/4/044028.
- Hirst, A., and S. Hastenrath (1983), Atmosphere-ocean mechanisms of climate anomalies in the Angola-tropical Atlantic sector, J. Phys. Oceanogr., 13(7), 1146-1157.



- lguchi, T., R. Meneghini, J. Awaka, T. Kozu, and K. Okamoto (2000), Rain profiling algorithm for TRMM precipitation radar data, Adv. Space Res., 25(5), 973-976, doi:10.1016/S0273-1177(99)00933-3.
- Julian, P. R., R. M. Chervin (1978), A study of the Southern Oscillation and Walker circulation phenomena, Mon. Weather Rev., 106,
- Kalb, C., A. Sciences, and S. L. City (2014), Parameterizing Total storm conduction currents derived in a global model, (June), 15–20.
- Keith, W. D., and C. P. R. Saunders (1990), Further laboratory studies of the charging of graupel during ice crystal interactions, Atmos. Res., 25(5), 445-464, doi:10.1016/0169-8095(90)90028-B.
- Kumar, P. R., and A. K. Kamra (2012), Variability of lightning activity in South/Southeast Asia during 1997-98 and 2002-03 El Niño/la Niña events, Atmos. Res., 118, 84-102, doi:10.1016/j.atmosres.2012.06.004.
- Liu, C., and E. J. Zipser (2009), "Warm rain" in the tropics: Seasonal and regional distributions based on 9 yr of TRMM data, J. Clim., 22(3), 767-779, doi:10.1175/2008JCLI2641.1.
- Liu, C., E. J. Zipser, D. J. Cecil, S. W. Nesbitt, and S. Sherwood (2008), A cloud and precipitation feature database from nine years of TRMM observations, J. Appl. Meteorol. Climatol., 47(10), 2712-2728, doi:10.1175/2008JAMC1890.1.
- Liu, C., E. R. Williams, E. J. Zipser, and G. Burns (2010), Diurnal variations of global thunderstorms and electrified shower clouds and their contribution to the global electrical circuit, J. Atmos. Sci., 67(2), 309-323, doi:10.1175/2009JAS3248.1.
- Liu, C., D. J. Cecil, E. J. Zipser, K. Kronfeld, and R. Robertson (2012), Relationships between lightning flash rates and radar reflectivity vertical structures in thunderstorms over the tropics and subtropics, J. Geophys. Res., 117, D06212, doi:10.1029/2011JD017123.
- MacGorman, D. R., W. D. Rust, P. Krehbiel, W. Rison, E. Bruning, and K. Wiens (2005), The electrical structure of two supercell storms during STEPS, Mon. Weather Rev., 133(9), 2583-2607, doi:10.1175/MWR2994.1.
- Mach, D. M., R. J. Blakeslee, M. G. Bateman, and J. C. Bailey (2009), Electric fields, conductivity, and estimated currents from aircraft overflights of electrified clouds, J. Geophys. Res., 114, D10204, doi:10.1029/2008JD011495.
- Mach, D. M., R. J. Blakeslee, M. G. Bateman, and J. C. Bailey (2010), Comparisons of total currents based on storm location, polarity, and flash rates derived from high-altitude aircraft overflights, J. Geophys. Res., 115, D03201, doi:10.1029/2009JD012240.
- Mach, D. M., R. J. Blakeslee, and M. G. Bateman (2011), Global electric circuit implications of combined aircraft storm electric current measurements and satellite-based diurnal lightning statistics, J. Geophys. Res., 116, D05201, doi:10.1029/2010JD014462.
- Markson, R. (2007), The global circuit intensity, Bull. Am. Meteorol. Soc., 88(2), 223-241.
- Nesbitt, S. W., and E. J. Zipser (2000), A census of precipitation features in the tropics using TRMM: Radar, ice scattering, and lightning observations, J. Clim., 13(23), 4087-4106, doi:10.1175/1520-0442(2000)013<4087:ACOPFI>2.0.CO;2.
- Orville, R. E., and D. W. Spencer (1979), Global lightning flash frequency, Mon. Weather Rev., 107, 934–943, doi:10.1175/1520-0493(1979) 107<0934:GLFF>2.0.CO;2.
- Petersen, W. A., H. J. Christian, and S. A. Rutledge (2005), TRMM observations of the global relationship between ice water content and lightning, Geophys. Res. Lett., 32, L14819, doi:10.1029/2005GL023236.
- Philander, S. G. (1989), El Niño, La Niña, and the Southern Oscillation, 293 pp., Academic Press, San Diego, Calif.
- Pinto, O., Jr., I. R. C. A. Pinto, and M. A. Ferro (2013), A study of the long-term variability of thunderstorm days in southeast Brazil, J. Geophys. Res. Atmos., 118, 5231-5246, doi:10.1002/jgrd.50282.
- Rasmusson, E. M., and J. M. Wallace (1983), Meterogical aspects of the El Niño, Sci. New Ser., 222(4629), 1195–1202, doi:10.1126/ science.222.4629.1195.
- Reynolds, S. E., M. Brook, and M. F. Gourley (1957), Thunderstorm charge separation, J. Meteorol., 14(5), 426-436, doi:10.1175/1520-0469 (1957)014<0426:TCS>2.0.CO:2.
- Richey, J., C. Nobre, and C. Deser (1989), Amazon River discharge and climate variability: 1903-1985, Science, 246(4926), 101.
- Roble, R. G., and I. Tzur (1986), The global atmospheric-electrical circuit, in The Earth's Electrical Environment, vol. 206, National Academy of Sciences Press, Washington, D. C.
- Ropelewski, C. F., and M. S. Halpert (1987), Global and regional scale precipitation patterns associated with the El Niño/Southern Oscillation, Mon. Weather Rev., 115(8), 1606–1626, doi:10.1175/1520-0493(1987)115<1606:GARSPP>2.0.CO;2.
- Sátori, G., and B. Zieger (1999), El Niňo related meridional oscillation of global lightning activity, Geophys. Res. Lett., 26, 1365, doi:10.1029/ 1999GL900264.
- Satori, G., E. Williams, and I. Lemperger (2009), Variability of global lightning activity on the ENSO time scale, Atmos. Res., 91(2-4), 500-507, doi:10.1016/j.atmosres.2008.06.014.
- Saunders, C. P. R. (2008), Charge separation mechanisms in clouds, Space Sci. Rev., 137, 335–353, doi:10.1007/s11214-008-9345-0.
- Saunders, C. P. R., and S. L. Peck (1998), Laboratory studies of the influence of the rime accretion rate on charge transfer during crystal/graupel collisions, J. Geophys. Res., 103, 13,949-13,956, doi:10.1029/97JD02644.
- Takahashi, T. (1978), Riming electrification as a charge generation mechanism in thunderstorms, J. Atmos. Sci., 35(8), 1536–1548, doi:10.1175/ 1520-0469(1978)035<1536:REAACG>2.0.CO;2.
- Takahashi, T., and K. Miyawaki (2002), Reexamination of riming electrification in a wind tunnel, J. Atmos. Sci., 59(5), 1018–1025, doi:10.1175/ 1520-0469(2002)059<1018:ROREIA>2.0.CO;2.
- Tinsley, B. A. (2000), Influence of solar wind on the global electric circuit, and inferred effects on cloud microphysics, temperature, and dynamics in the troposphere, Space Sci. Rev., 94(1-2), 231-258.
- Trenberth, K. (1997), The definition of El Niño, Bull. Am. Meteorol. Soc., 78(12), 2771-2777, doi:10.1175/1520-0477(1997)078<2771: TDOENO>2.0.CO:2.
- Whipple, F. J. W. (1929), On the association of the diurnal variation of the electric potential gradient in fine weather with the distribution of thunderstorms over the globe, Q. J. R. Meteorol. Soc., 55, 351–361.
- Waliser, D., and C. Gautier (1993), Waliser and gautier, J. Clim., 6(11), 2162-2173.
- Williams, E. R., and S. J. Heckman (1993), Diurnal variation of negative charge on the Earth, J. Geophys. Res., 98, 5221-5234.
- Williams, E. R. (1994), Global circuit response to seasonal variations in global surface air temperature, Mon. Weather Rev., 122(8), 1917–1929, doi:10.1175/1520-0493(1994)122<1917:GCRTSV>2.0.CO;2.
- Williams, E., and S. Stanfill (2002), The physical origin of the land-ocean contrast in lightning activity, Comptes Rendus Phys., 3(10), 1277–1292, doi:10.1016/S1631-0705(02)01407-X.
- Williams, E. R., and G. Sátori (2004), Lightning, thermodynamic and hydrological comparison of the two tropical continental chimneys, J. Atmos. Sol. Terr. Phys., 66(13-14 SPEC. ISS), 1213-1231, doi:10.1016/j.jastp.2004.05.015.
- Williams, E. R. (2009), The global electrical circuit: A review, Atmos. Res., 91(2-4), 140-152, doi:10.1016/j.atmosres.2008.05.018.
- Williams, E., and E. Mareev (2014), Recent progress on the global electrical circuit, Atmos. Res., 135-136, 208-227, doi:10.1016/j. atmosres.2013.05.015.



# **Journal of Geophysical Research: Atmospheres**

- Wilson, C. T. R. (1920), Investigations on lightning discharges and the electric field of thunderstorms, *Philos. Trans. R. Soc. London, Ser. A.*, 221, 73–115.
- Workman, E. J., and S. E. Reynolds (1950), Electrical phenomena occurring during the freezing of dilute aqueous solutions and their possible relationship to thunderstorm electricity, *Phys. Rev.*, 78, 254–259.
- Yu, J.-Y., H.-Y. Kao, T. Lee, and S. T. Kim (2010), Subsurface ocean temperature indices for central-Pacific and eastern-Pacific types of El Nino and La Nina events, *Theor. Appl. Climatol.*, 103, 337–344, doi:10.1007/s00704-010-0307-6.
- Zipser, E. J., D. J. Cecil, C. Liu, S. W. Nesbitt, and D. P. Yorty (2006), Where are the most: Intense thunderstorms on Earth?, Bull. Am. Meteorol. Soc., 87(8), 1057–1071, doi:10.1175/BAMS-87-8-1057.